Applied Catalysis B: Environmental 248 (2019) 202–210

Contents lists available at ScienceDirect

Applied Catalysis B: Environmental

journal homepage: www.elsevier.com/locate/apcatb

Metal-organic framework derived Co_3O_4/MoS_2 heterostructure for efficient bifunctional electrocatalysts for oxygen evolution reaction and hydrogen evolution reaction

Alagan Muthurasu[a], Viruthasalam Maruthapandian[c], Hak Yong Kim[a,b,*]

[a] Department of BIN Convergence Technology, Chonbuk National University, Republic of Korea
[b] Department of Organic Materials and Fiber Engineering, Chonbuk National University, Jeonju 561-756, Republic of Korea
[c] CSIR - Central Electrochemical Research Institutes, Karaikudi, 630 003, Tamilnadu, India

ARTICLE INFO

Keywords:
Metal-organic framework
Bifunctional
Catalysts
Heterostructure and synergistic

ABSTRACT

Fabrication of highly efficient, sustainable and low-cost nonprecious metal oxide for oxygen evolution reaction (OER) and hydrogen evolution reaction (HER) is exceedingly challenging and warranted for overall water splitting. Herein, we synthesized cobalt nanoleaves metal-organic framed work (MOF) on nickel foam substrate with uniform growth. After calcination of Co-MOF, molybdenum disulfide nanosheets is grown by a facial hydrothermal method. The as-prepared heterostructure (Co_3O_4/MoS_2) can act as bifunctional electrocatalysts for overall water splitting. Under optimized condition, synthesized Co_3O_4/MoS_2 heterostructure catalyst exhibited excellent catalytic activity for both OER and HER in 1 M KOH solution with a current density of 20 mA cm^{-2} at overpotential of 230 mV for OER and 205 mV for HER (@ j = 10 mA cm^{-2}) and Tafel slopes of 45 and 98 mV dec^{-1}, respectively. The superior catalytic activity for both OER and HER arises from the unique heterostructure of Co_3O_4/MoS_2 and the synergistic effects of Co_3O_4 and MoS_2.

1. Introduction

The substantial anxieties of fossil fuel depletion and environmental consequences of exponential CO_2 emissions have motivated significant efforts to develop a new renewable material of sufficient scale to replace fossil fuels and to meet rising global energy demand [1–5]. Among them, electrochemical water splitting has been intensively studied for obtaining hydrogen fuel production, which is one of the most significant approaches for clean and scalable energy substitutes [6–9]. This efficient electrochemical process and electrocatalysts success relies on the development of hydrogen evolution reaction (HER) and the oxygen evolution reaction (OER) with comparable or even better efficiencies than those of noble metal-based catalysts already known, eventually minimize the overpotential, achieve fast kinetics, stability and reduce fabrication cost for practical applications [10,11]. Precious metal and their oxide based electrocatalysts such as IrO_2, RuO_2, and Pt/C have been considered as the benchmark catalysts, which possesses superior performance in OER and HER. However, their high cost and rare availability greatly impede their widespread applications [12–14]. Therefore, in recent year enormous efforts have been devoted to exploiting non-precious metal electrocatalysts consisting of earth-abundant materials as a cost-effective alternative for the OER and HER [15,16]. Transition metal-based electrocatalysts have recently emerged as plausible alternatives for precious metal catalysts. There are several approaches that have been developed recently for the synthesis of non-precious metal catalysts. For instance, first-row transition metal alloys [17], sulfides [18,19], selenides [20,21], phosphides [22–24], nitrides [25–27], hydroxides [28,29], oxides [30,31] have been considered as a promising bifunctional electrode material for HER and OER. Water electrolysis, such as OER and HER catalysts are generally tested in different electrolyte media [32]. However, to accomplish overall water splitting, the coupling of HER and OER catalysts in the same electrolyte still remains a huge exigent task owing to a wide pH range mismatch [33,34]. Alkaline water splitting is being developed as a strong candidate for commercialization towards mass hydrogen production. Therefore, highly efficient bifunctional electrocatalysts for overall water splitting in alkaline conditions certainly have advantages for water splitting devices.

Metal-organic frameworks (MOFs) represent a class of organic-inorganic hybrid materials that have attracted much attention due to their controllable structures and tunable pore sizes [35–37]. These are being constructed by strong bonds between metal ion clusters as nodes

* Corresponding author.
E-mail address: khy@jbnu.ac.kr (H.Y. Kim).

https://doi.org/10.1016/j.apcatb.2019.02.014
Received 23 July 2018; Received in revised form 30 January 2019; Accepted 9 February 2019
Available online 10 February 2019
0926-3373/ © 2019 Elsevier B.V. All rights reserved.

and multitopic organic linkers as spacers [38]. The most usual synthetic method for MOFs under mild conditions are solvothermal [39], electrochemical [40], microwaves [41], and mechanochemical [42] methods. Due to their well-known structural characterizations, including high porosity, specific surface area, tunable pore structure and easy functionalization, MOFs pave way for their potential application in various fields, such as gas adsorption/separation [43], magnetism [44], optoelectronics [45], proton conductivity [46], and biomedicine [47]. In particular, MOFs has been explored for HER and OER catalysis as one of the promising applications in recent years [2,35,48,49]. Most importantly, MOF route for synthesized metal oxide exhibits excellent electrochemical performance towards water splitting reaction and other catalytic reactions. Metal ions and organic ligands in MOFs demonstrate catalytically active center for electrocatalytic performance towards OER and HER due to their porosity [2,35,50]. In addition to that, direct carbonization of MOF leads to the conversion of the resultant catalyst by self-sacrifice methods and it offers porous unique morphologically controlled derivatives as well as large surface and catalytic active area [51]. These MOF derived functional materials usually exhibit remarkable electrical conductivity, chemical stability, and catalytic efficiency [35].

MoS_2 based electrocatalysts have been extensively examined as one of the most promising non-noble metal catalysts for the electrochemical generation of hydrogen from water due to their abundance and low cost [11,52,53]. However, bulk MoS_2 exhibits less HER activity due to large internal resistance and lack of active edge sites [54,55]. Recently, experimental and computational studies revealed that the HER activity of MoS_2 originates from under coordinated Mo-S sites along the MoS_2 edges which is similar to that of Pt [56]. Hence, for the enhancement of catalytic activity achieved by a surface defective engineering method and the addition of carbon-based conductive additives with MoS_2 and hybrid with MXenes [9,53,57–59]. For OER electrocatalysts, the unsaturated metal particles on oxide surface are of crucial importance for water oxidation because of their strong chemisorption of the formed OH^- and oxygen-containing intermediates [35]. Therefore, rational designing of novel heterostructure to fulfill the synergy in heterostructure and increase the binding affinities of both hydrogen and oxygen-containing intermediates is of the extremely great advantage of improving the activity of overall water splitting [11,60]. From this perspective, fabrication of such a heterostructure paves a novel path for enhancing the overall water splitting. Despite that, these strategies have been efficiently used to build three-dimensional (3D) networks which are usually complex due to their multiple-step synthesis. In situ growth of metal oxides over the metallic 3D architectures offers exceptional conductivity for the efficient electron transport for redox reactions due to binder free adhesive nature, higher stability because of the metal oxide and metal interaction. In addition to these, the porosity of substrates offers more actives sites and surface area in connection with the grown catalysts over the surface, higher mass diffusion owing to highly porous nature especially for the gas evolution reactions, structural and chemical stability [8,61–63]. Hence, in situ growth and surface modification of metallic substrates is still an evolving area diverge in the electrocatalytic applications.

Herein, we have employed the interface engineering to construct novel hierarchical structures of MoS_2nanosheets wrapped MOF based Co_3O_4 nano leaves heterostructures grown on nickel foam (Co_3O_4/MoS_2). Firstly, well-aligned Co-MOF nano leaves that are grown by in situ liquid deposition method and then annealing in air atmosphere. The resultant Co_3O_4 nano leaves surface is being decorated with layers of MoS_2 nanosheet that is directly grown by a facile hydrothermal process. The obtained novel Co_3O_4/MoS_2 heterostructure catalyst system exhibits a notable enhancement in HER and OER activities compared to pure Co_3O_4 and MoS_2 nanostructures. Unique three dimensional (3D) layered MoS_2 nanostructures could offer more active sites at the heterointerface. As predicted, Co_3O_4/MoS_2 heterostructure catalyst exhibited lower overpotential of 230 mV for the OER (@ 20 mA cm^{-2}) and 205 mV (@ 10 mA cm^{-2}) for the HER together with excellent stability in alkaline electrolytes. We have emphasized that their higher performance towards both OER and HER activity is mainly attributed to a synergistic effect between the Co_3O_4 nano leaves and MoS_2 nanosheet. This work reveals the integration of non-noble metal based robust electrocatalysts for overall water splitting application.

2. Experimental section

2.1. Chemicals

Analytical grade cobalt nitrate hexahydrate ($Co(NO_3)_2.6H_2O$), and 2-methylimidazole (Hmim) were purchased from Sigma Aldrich. Sodium molybdate ($Na_2MoO_4{\cdot}2H_2O$.) was purchased from Showa Chemical Co. LTD. Thiourea (CH_4N_2S, TU) was purchased from Samchun Chemicals. Prior to use, the Ni foam substrate (2 × 2 cm^2) was pretreated with 6 M HCl for 30 min to remove the surface NiO layer and then washed with deionized water and absolute ethanol for 3–5 times respectively. All other chemicals were used as without any further purification.

2.2. Synthesis of leaf-like Co-MOF and Co_3O_4/MoS_2 grown on Ni foam

In a distinctive experiment, 0.3 M of 2-methylimidazole (Hmim) and 0.06 M of $Co(NO_3)_2$. $6H_2O$ were dissolved individually in 50 ml deionized water with 30 min of magnetic stirring at room temperature. After 15 min of magnetic stirring, $Co(NO_3)_2.6H_2O$ solution was carefully transferred into the Hmim solution quickly and then a piece of thoroughly cleaned Ni foam (2 cm^2) was completely immersed in the above-mentioned solution and kept for 1 h. After that, the product supported Ni foam was washed with deionized water several times and dried at a temperature of 60 °C in the electric oven overnight. Finally, the as-grown Ni foam was pyrolyzed at 300 °C in an air atmosphere for 1 h at a heating rate of 1 °C min^{-1} to obtain Co_3O_4 nano leaves supported on the Ni foam. Then, the as-prepared Co_3O_4 nano leaves supported Ni foam was immersed in a 15 ml DMF solution containing MoS_2, disperesed in ultrasonication for several hours. The mixture was placed into a 100 ml Teflon-lined stainless steel autoclave, and the autoclave was tightly sealed and kept at 200 °C for 10 h. Aftercooling down to room temperature, the as-grown Co_3O_4/MoS_2 Ni foam was washed several times with deionized water followed by ethanol and dried at 60 °C overnight. Co_3O_4 nano leaves supported on the Ni foam was prepared with the same procedures, 0.3 M of 2-methylimidazole (Hmim) and 0.06 M of $Co(NO_3)_2$. $6H_2O$ were mixed with 40 ml water and stirred 15 min forming a homogeneous solution. Subsequently, precleaned Ni foam was immersed in the above solution for 1 h and washed with plenty of Millipore water and dried at 60 °C to get the Co-MOF nano leaves. Finally, Co-MOF grown on Ni foam was pyrolyzed at 300 °C in an air atmosphere for 1 h at a heating rate of 1 °C min^{-1} to obtain Co_3O_4 nano leaves supported on the Ni foam. Similarly, MoS_2 nanosheet was grown on nickel foam under the same condition, except the growth of Co-MOF on nickel foam, the typical procedure, precleaned Ni foam was immersed in a 15 ml DMF solution containing 2 mM sodium molybdate ($Na_2MoO_4{\cdot}2H_2O$) and 8 mM thiourea (CH_4N_2S). After a hydrothermal reaction at 200 °C for 24 h, MoS_2 nanosheet was on the nickel foam was obtained.

2.3. Material characterizations

The surface morphology, elemental composition (energy dispersive X-ray (EDX)) and elemental mapping of the as-synthesized heterostructure was detected using a scanning electron microscope (SEM) (Hitachi S-7400, Japan). TEM images were recorded with a JEOL JEM 2010 with an operating of 200 kV (JEOL Ltd, Japan). The crystallographic phases of the samples were characterized by using a Rigaku X-ray diffractometer (Rigaku Co., Japan) using Cu Ka radiation with a

wavelength of 1.540 Å and a 2θ value ranging from 10 to 80°. The electrochemical measurements were tested by conventional three-electrode configuration using VersaSTAT 4 electrochemical analyzers at room temperature.

2.4. Electrochemical measurements of electrocatalysts

The electrochemical measurements including EIS and LSV were carried out by using a conventional three-electrode system comprising of a platinum wire and sat Ag/AgCl as the auxiliary and reference electrode respectively. The as-prepared Co_3O_4 nano leaves grown on Ni and Co_3O_4/MoS_2 foam was used as the working electrode with a geometric area of (1 cm^2), without adding any conductive additive and binder. For comparison, benchmark OER and HER catalyst under identical conditions, IrO_2 and Pt/C were used on the Ni foam which was prepared by mixing the catalyst with PVDF binder in NMP solvent. In all the cases catalyst loading on the Ni foam substrate was around 2 mg cm^{-2}. The obtained current values were normalized with respect to the geometric surface area to get its respective current density. All the potential data reported in this work are in accordance with the reversible hydrogen electrode (RHE) and calibration parameter was accomplished according to the Nernst equation given by $E_{RHE} = E_{Ag/AgCl} + 0.059 \times pH + 0.197$ V. The polarization curves were obtained in 1.0 M KOH using linear sweep voltammetry (LSV) with a scan rate of 10 mV s^{-1}. Tafel polarization studies were performed to determine the kinetic parameters accompanying with polarization curves. Electrochemical Impedance spectra were obtained at frequencies ranging from 100 kHz to 0.01 Hz using amplitude signal of 5 mV with the desired overpotential of OER and HER conditions. The long term durability test was performed using chronoamperometry measurement. Polarization curves depict that the current values are corrected against the ohmic potential drop (iR) measured from the ESI. Turn over frequency (TOF) of catalysts calculated at 300 mV and 250 mV of overpotential respectively for the OER and HER using the relation of TOF = (J/n × F), whereJ is the current density in A cm^{-2}, n is the number of electrons transferred in the reaction (2 and 4 for HER and OER respectively), F is the Faraday constant (96,485 C mol^{-1}).

3. Results and discussion

3.1. Synthesis and characterization of Co_3O_4/MoS_2 heterostructure

The structural morphology of as-prepared materials was investigated by employing scanning electron microscopy (SEM) and the images are shown in Fig. S1 in ESI. As shown, the Co MOF has grown uniformly on the nickel foam substrate with leaf-like structure. The SEM images indicate that the surface of the nano leaf has a smooth surface with an average thickness of each nano leaf of Co-MOF to be 100–150 nm. The Co_3O_4 can be prepared by calcinating (Fig. 1A) Co-MOF at 300 °C in air atmosphere. In Fig. 1B it is clearly revealed that even after high-temperature calcination, the size homogeneity and leaf-like morphology of Co_3O_4 are well retained. After facile hydrothermal reaction, the surface of the Co_3O_4 nano leaves are uniformly covered by MoS_2 nanosheet (Fig. 1C) forming a three-dimensional (3D) hierarchical network. We can barely see the Co_3O_4 nano leaves unravelling from the MoS_2 nanosheet (Fig. 1D), implying a strong interaction between Co_3O_4 nano leaves and MoS_2 nanosheet. This gives assurance for the high electrochemical performance towards OER and HER. The elemental mapping (Fig. 1E-J) showed that Mo, S, Co, and O are distributed uniformly in the heterostructure; Energy-dispersive X-ray spectroscopy (EDX) results show that the heterostructure mainly consists of (Fig. 1K and 1 L) stoichiometric composition of Co, Mo, O, C and S. It reveals that the stoichiometric composition of Co_3O_4/MoS_2 heterostructure displays the stoichiometric ratio of Co, Mo, O, C and S to be 24.95%, 17.98%, 30.08%, 6.89%, and 20.1% respectively. Transmission electron microscope (TEM) image (Fig. 1M) gives unique possibilities to gain insights into the morphology and structure of resultant heterostructure. This suggested that the as-prepared Co_3O_4/MoS_2 heterostructure exhibit leaf-like shape covered by thin layers of MoS_2 nanosheet. Fig. 1N depicts selected area diffraction (SAED) of Co_3O_4/MoS_2 heterostructure has been indexed (Fd3m, card No. 74-1657) and obtained results revealed that the as-prepared heterostructure is polycrystalline in nature. Fig. 1O shows a lattice fringe pattern of Co_3O_4/MoS_2 heterostructure displays the interplanar spacings of 0.46 nm and 0.62 nm, corresponding to the (111) and (002) planes of the spinel Co_3O_4 nano leaves and MoS_2 nanosheet respectively. Fig. S2 in SI indicates the digital photographic image of bare Nickel foam (A), Co-MOF (B) and Co_3O_4/MoS_2 (C) heterostructure. These results support that MoS_2 nanosheet subunit is grown vertically on the surface of Co_3O_4 with their fully exposed abundant active site edges [35,56].

Crystalline structure and phase purity of the as-prepared, calcined product and resultant heterostructure of Co_3O_4/MoS_2 was analyzed using X-ray diffraction (XRD) studies. The XRD pattern of the as-prepared Co-MOF (Fig. S3 in ESI) nano leaves is in good agreement with the previous reports [64]. The products after the calcination of Co-MOF is shown in Fig. 2. XRD pattern of MoS_2 (a), Co_3O_4 (b), and hydrothermally prepared Co_3O_4/MoS_2 heterostructure (c) catalysts confirms the existence of oxide formation onto the layered MoS_2 nanosheets which is fully covered on the surface of Co_3O_4 nano leaves. The diffraction peaks at 14.05°, 33.28°, 39.0° and 58.50° are designed for the (002), (100), (103) and (110) planes of MoS_2, respectively (JCPDS No. 37-1492) [65]. Similarly, prominent peaks at 2θ values of 19.2°, 31.2°, 37.1°, 45.1°, 59.7°, and 65.6° respectively assigned to (111), (220), (111), (311), (400), (511) and (440) planes of Co_3O_4. In addition to that, it should be noted that three characteristic peaks at 2θ = 44.5°, 51.8°, and 76.4° arise from the Ni foam substrate (JCPDS No. 65-2865) [56]. Except for these three typical peaks of Ni foam, other diffraction peaks in XRD patterns are in good concordance with Co_3O_4 of face-centered cubic (fcc) phase of pristine Co_3O_4 (Fd3m, card No. 74-1657) [66] and no other miscellaneous peaks were found in the samples indicating that the high purity and crystallinity of the as-prepared Co_3O_4/MoS_2 heterostructure.

Furthermore, X-ray photoelectron spectroscopy (XPS) was carried out to investigate the chemical and electronic states of the interfacial surface. The XPS survey spectrum (Fig. S4 in ESI) shows typical signals for the Co, Mo, S, C and O elements (compatible with EDS analysis), and the resulting high-resolution scans of distinct elements are shown in Fig. 3. The binding energy of Co_3O_4 exhibits two strong peaks centred at 780.1 eV and 795.6 eV, and two shakeup satellite peaks which are assigned to the binding energy of Co $2p_{2/3}$ and Co $2p_{1/2}$ spin-orbital coupling respectively [66,67]. In the deconvoluted (Fig. 3A) Co $2p_{2/3}$ high-resolution spectra region, the two peaks located at 780.1 eV and 782.0 eV which are ascribed to the binding energy of Co^{3+} and Co^{2+} respectively. Similarly, two peaks in Co $2p_{1/2}$ deconvolution region located at 795.7 eV and 796.8 eV have similarity with that of the Co $2p_{3/2}$ deconvolution spectra. Furthermore, the energy separation between the Co $2p_{3/2}$ peak and the Co $2p_{1/2}$ peak is approximately 15.5 eV which is characteristic of the Co $2p_{3/2}$ and Co $2p_{1/2}$ orbitals of Co_3O_4 (Fig. 3A), respectively [66,67]. In contrast, the binding energy values of Co shift positively about 0.3 eV after the MoS_2 wrapped onto the Co_3O_4 associated with that of pure Co_3O_4 nano leaves, suggesting that strong electronic coupling of MoS_2 and Co_3O_4. [68]. The high-resolution Mo, 3d spectrum (Fig. 3B) could be deconvoluted into Mo $3d_{5/2}$ (229.1 eV) and Mo $3d_{3/2}$ (232.2 eV), corresponds to the higher oxidation state of Mo approximating to +6 [52]. Moreover, the peak at 226.8 eV could be assigned to S 2 s [65]. Nevertheless, after constructing with heterostructure the binding energy values of Mo $3d_{5/2}$ (229.4 eV) and Mo $3d_{3/2}$ (232.5 eV) in the Co_3O_4/MoS_2 shifted of 0.3 eV positive shifts comparable to that in bare MoS_2. Similarly, the sulfur S 2p (162.5 eV) spectrum of Co_3O_4/MoS_2 heterostructures exhibits a negative shift of 0.4 eV (Fig. 3C) compared to that of bare MoS_2

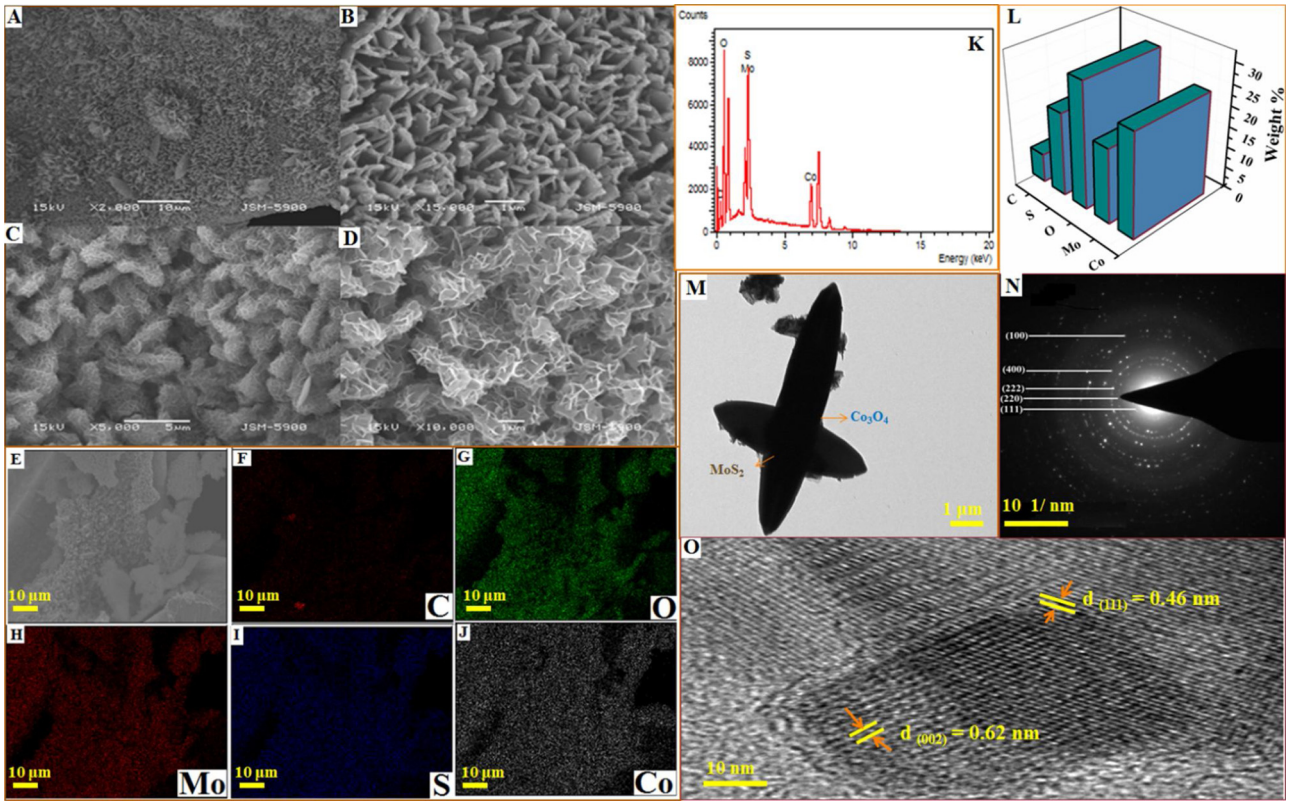

Fig. 1. SEM images of MOF based Co_3O_4 nano leaves (A) at low and (B) high magnification. (C) Low and high (D) magnification SEM images of the Co_3O_4/MoS_2 heterostructure. (E) Elemental mapping images of C (F), O (G), Mo (H), S (I) and Co (J) for Co_3O_4/MoS_2 heterostructure. EDX spectrum (K) and (L) elemental composition of Co_3O_4/MoS_2 heterostructure obtained from the EDX spectrum (K). (M) TEM image of Co_3O_4/MoS_2 heterostructure. (N) Selected area electron diffraction (SAED) pattern of the resultant Co_3O_4/MoS_2 heterostructure and (O) displays the lattice fringe spacing of the resultant Co_3O_4/MoS_2 heterostructure found from HRTEM studies.

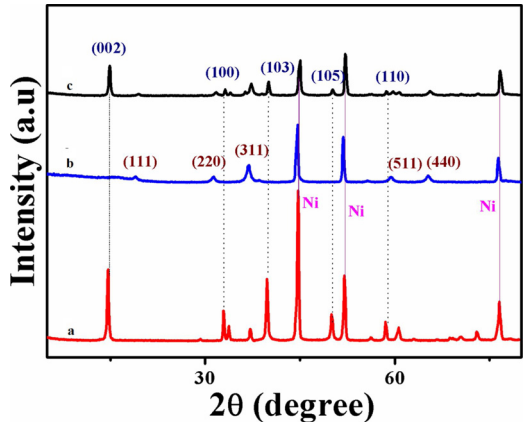

Fig. 2. XRD pattern of (a) MoS_2 nanosheet, (b) MOF based Co_3O_4 nano leaves and (C) Co_3O_4/MoS_2 heterostructure on Ni foam respectively.

(sulfur S 2p located the peaks centred at 162.1 eV which is fitted to S $2p_{3/2}$) indicates an increased electron density of heterostructures hence the adsorption ability to H* intermediate is dramatically enhanced [11,69]. Fig. 3D shows the high-resolution O 1 s spectrum could be matched with oxygen peak observed at 533.7 eV associated with oxygen in hydroxyl groups, and surface lattice oxygen bond physi/chemisorbed water molecules on the surface respectively [52].

3.2. Electrocatalytic activity of Co_3O_4/MoS_2 heterostructure

3.2.1. OER catalytic activity of Co_3O_4/MoS_2 heterostructure

Requisite to accomplish MOF oriented metal oxide with the uniformly covered 3D distribution of MoS_2 nanosheet catalyst owing to its extraordinary availability and good stability could gain potential application of electrocatalysts. The OER activity of the bifunctional Co_3O_4/MoS_2heterostructure was first assessed by linear sweep voltammetric (LSV) measurement between the potential window of 1.1 and 1.7 V vs. reversible hydrogen electrode (RHE) in 1 M KOH by a three-electrode electrochemical setup. Catalysts modified electrode exhibits a pair of redox peaks at 1.3–1.4 V vs. RHE, which ascribed to Co^{2+}/Co^{3+} redox couple of Co_3O_4 (Fig. S5 in ESI). A small hump prior to the onset of OER, designate to the Co^{3+}/Co^{4+}. The formation of these two species to create specific catalytic phase for OER. The different active site, such as Co^{3+} and Co^{4+} leads to the adsorption of OH^- ion during OER in alkaline medium. Apart from these active sites, exposing the crystalline plane to the electrolyte can play a crucial role in OER [30,70]. The electrocatalytic OER activities of the Co_3O_4/MoS_2 heterostructures along with the activity of other materials such as Ni foam, Co_3O_4, MoS_2 nanosheet, and commercial IrO_2 were investigated using LSV at a scan rate of 10 mV s^{-1} as depicted in Fig. 4A. Compared to the individual materials, polarization curve for the Co_3O_4/MoS_2 heterostructure catalysts achieved a low overpotential (η) of 230 mV at the current density of 20 mA cm^{-2}, which is a higher metric relevant to the solar fuel system (10 mA cm^{-2} for 12.3% efficiency of solar to fuel conversion) that are commonly used to evaluate the activity of catalysts [26]. This value is lower than that of Co_3O_4 (320 mV), MoS_2 (560 mV) and IrO_2 (260 mV) bare Ni foam (370 mV) individual entities; it is comparable to that of benchmark catalyst's (IrO_2) overpotential. Additionally, another significant parameter of comparative catalytic activity characteristics of TOF was calculated at 300 mV of overpotential. Co_3O_4/MoS_2 showed 1.4 times higher than compared to individual and benchmark catalysts (Table S1 in ESI). Corresponding Tafel plots were

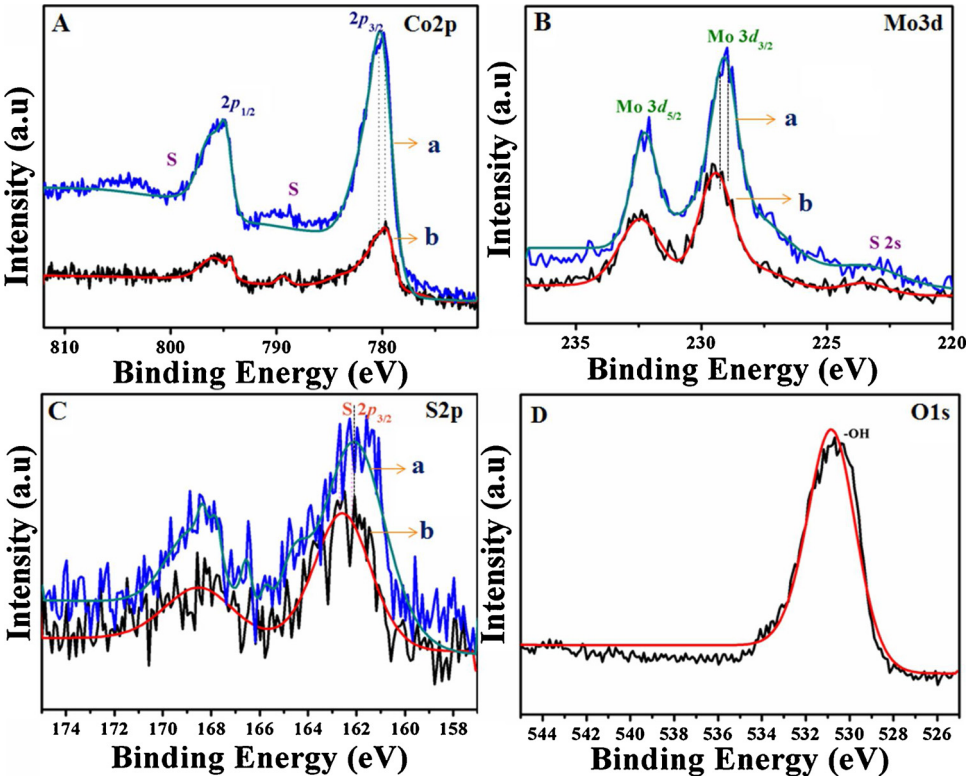

Fig. 3. High-resolution XP spectra of (A) Co 2p (a) Co_3O_4, (B) Mo 3d (a) MoS_2, (C) S 2p (a) MoS_2, and (D) O 1 s in (b) Co_3O_4/MoS_2 heterostructure respectively.

drawn to further study the mechanistic insights into OER kinetics amiable through approaching Tafel slopes from polarization curves. The linear regions of Tafel plots were fitted to the polarization curve in a low potential region: η = blogj + a, where η is the overpotential, j is the current density, a is constant and b is the Tafel slope. It should be noted that Co_3O_4/MoS_2 heterostructure displayed Tafel slope of only 45 mV dec^{-1} (Fig. 4B) which was prominently smaller than Co_3O_4 (94 mV dec^{-1}) and MoS_2 (298 mV dec^{-1}) and Ni foam (120 mV dec^{-1}) IrO_2 (68 mV dec^{-1}) (Fig. S6 in ESI) respectively. These results reveal that after integration of MoS_2 nanosheet on Co_3O_4 nano leaves, the overpotential and Tafel slope values (Fig. 4C) was sharply reduced because MoS_2 nanosheet shortens the electron and ions transportation/diffusion bath as a result kinetics of electrochemical oxidation of OER increased [54]. The long-term stability is another important criteria for OER electrocatalysts [54]. To assess the long-term water oxidation stability, it was tested at a constant applied potential of 1.53 V vs RHE for 13 h. The OER activity remained unchanged under the operating conditions and it deleverd almost constant current density of 20 mA cm^{-2}. (Fig. 4D) [26]. Moreover, Co_3O_4/MoS_2 heterostructure was tested by taking CV curves for 500 cycles at a scan rate of 50 mV s^{-1} as shown in Fig. S7 in ESI. There was negligible degradation after continuous polarization of 500 cycles, suggesting that excellent stability under OER conditions. Meanwhile, electrochemical impedance spectroscopy (EIS) techniques of Co_3O_4/MoS_2, Co_3O_4, MoS_2, and Ni foam were demonstrated in 1 M KOH electrolyte (Fig. 4E). The Co_3O_4/MoS_2 heterostructure catalyst shows the lowest charge transfer resistance (R_{ct}) indicated by the formation of the very small semicircle in the high-frequency region than that of the pristine MoS_2 and Co_3O_4 catalysts, the obtained values of R_{ct} are 3.5 Ω, 11.55 Ω, 20.19 Ω and 29.19 Ω for of Co_3O_4/MoS_2, Co_3O_4, MoS_2, and Ni foam respectively at the overpotential of 300 mV. Revealing a remarkably improved conductivity and enhanced charge transfer process for Co_3O_4/MoS_2 heterostructure catalyst. The R_{ct} values are consistent with the trends of measured OER activities [71].

The electrochemical surface area (ECSA) of Co_3O_4/MoS_2 heterostructure is evaluated by cyclic voltammetry (CV). The electrochemical double-layer capacitance (C_{dl}) is measured from non-Faradaic regions typically in the range of 1.0 to 1.2 V vs. RHE. It can be clearly seen that CVs do not show any visible peak formation, suggesting an electrical double layer capacitor (Fig. S8 in ESI). Fig. 4F shows the C_{dl} is calculated by current density against the potential of scan rate and the obtained slopes of these fitting lines (C_{dl}) are in good agreement with an assessment of the ECSA [66]. The C_{dl} of the Co_3O_4/MoS_2 heterostructure is about 6.7 m F cm^{-2}, which is 4 times higher than Co_3O_4 (about 1.66 m F cm^{-2}). Thus, the Co_3O_4/MoS_2 heterostructure catalyst with larger C_{dl} can afford more access to the electrolyte through its exposed active sites and significantly subsidize to its electrocatalytic activity towards OER by the adsorption and desorption of reactive intermediates.

3.2.2. HER catalytic activity of Co_3O_4/MoS_2 heterostructure

The HER catalytic performance of the same Co_3O_4/MoS_2 heterostructure catalyst was next investigated by applying typical iR-corrected polarization curves obtained at a scan rate of 10 mV s^{-1} in the standard three electrode electrochemical cell using 1 M KOH solution. Besides, with a Co_3O_4/MoS_2 heterostructure, HER activity of reference materials such as Co_3O_4, MoS_2, Ni foam and along with that of commercial Pt/C (20 wt %) was also tested under the same condition which is shown in Fig. 5A. As expected, Pt/C shows the best catalytic activity with an overpotential of 42 mV at 10 mA cm^{-2} current density, in comparison to other individual materials. But the scarcity of these materials limits their practical applications. The HER catalytic performance of Co_3O_4/MoS_2 heterostructure exhibits lower overpotential of 205 mV to drive 10 mA cm^{-2}. On the contrary, Co_3O_4, MoS_2, Ni foam exhibited the minimum catalytic activity and required overpotential of 254, 215 and 301 mV to attain a current density of 10 mA cm^{-2}. Similar to the OER catalytic activity of TOF, for HER TOF was calculated at 250 mV of overpotential. Contrast with OER TOF, Co_3O_4/MoS_2 was found higher and almost half TOF of benchmark Pt/C catalyst than compared to others Table S1 in ESI. Further to deeply understand the

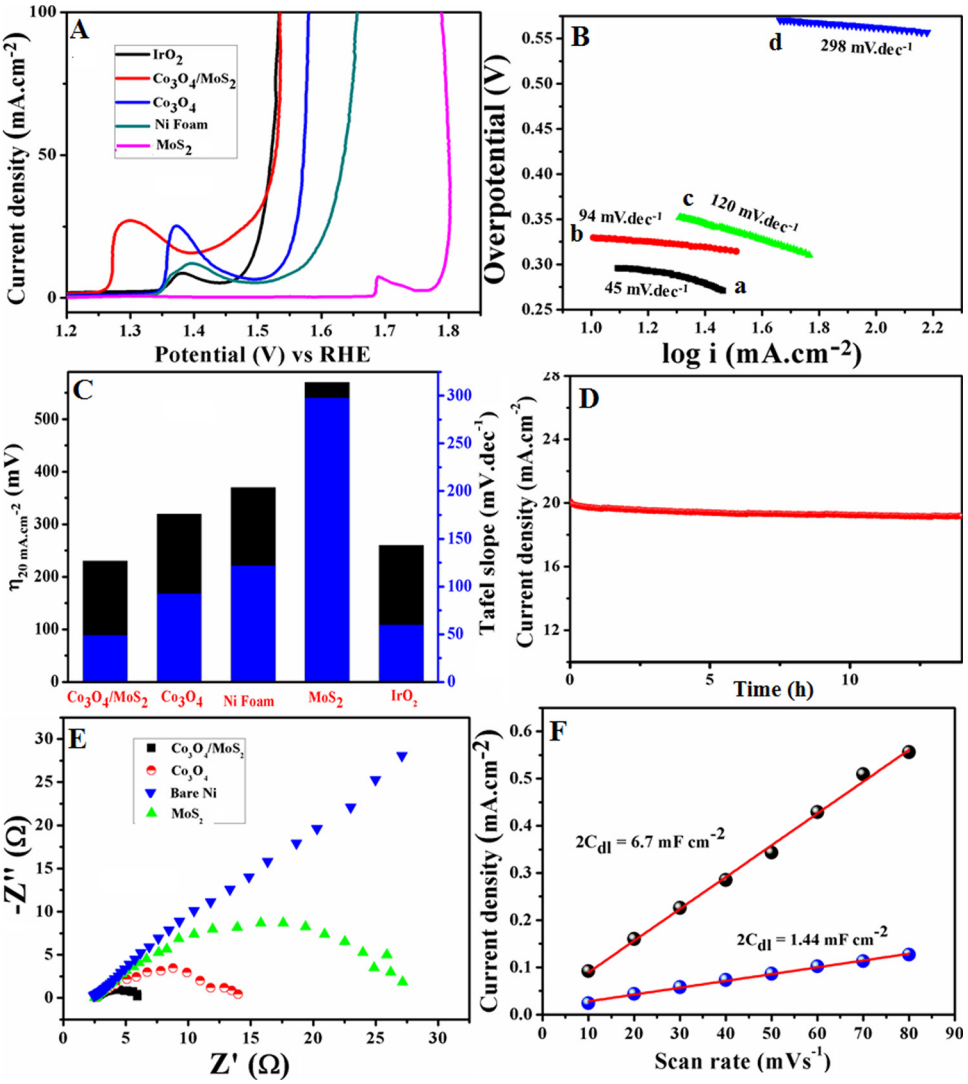

Fig. 4. (A) LSV curves of IrO_2, Co_3O_4 /MoS_2, Co_3O_4, MoS_2 and Ni foam for OER catalysts in 1.0 M KOH solution. (B) corresponding Tafel plots of the data derived from (A) whereas a) Co_3O_4/MoS_2, b) Co_3O_4 c) Ni foam and d) MoS_2. (C) OER catalytic activity comparison of the over potential (@ 20 mA cm^{-2}) and Tafel slope of catalysts. (D) CA plot of the Co_3O_4/MoS_2 heterostructure electrode at a constant applied potential of 1.46 V vs RHE. (E) EIS plots of different catalyst electrodes at 300 mV over potential. (F). Electrochemical active surface area (ECSA) analysis for the linear fitting of difference in current density ($\Delta j = j_a - j_c$) at 1.1 V vs RHE with respect to scan rate for (a) Co_3O_4/MoS_2 and (b) Co_3O_4.

electrocatalytic HER kinetics of the prepared materials Tafel slopes were studied as shown in Fig. 5B. The Tafel slopes of 98, 128, 199, and 258 mV dec^{-1} were achieved for Co_3O_4/MoS_2, MoS_2, Co_3O_4, and Ni foam respectively. The lower Tafel slope value of Co_3O_4/MoS_2 heterostructure catalyst indicates the Volmer–Heyrovsky reaction pathway is operative with the superior HER kinetics of desorption of hydrogen (Volmer step) and rapid increase of catalytic current towards the HER catalytic activity [3,61]. This trend is consistent with electrochemical impedance spectroscopy (EIS), EIS techniques demonstrated that (Fig. 5C) electrocatalysts of Co_3O_4/MoS_2, MoS_2, Co_3O_4, and Ni foam obtained in 1 M KOH electrolyte measured at an overpotential of 100 mV. Co_3O_4/MoS_2 heterostructure exhibits lower charge transfer resistance (R_{ct}) than the other individual entities as similar to OER, implies a facile charge-transfer process. Thus, it speeds up the faster reaction rate in case of HER kinetics process, hence it reduces HER overpotential. Similarly, the long-term stability of the Co_3O_4/MoS_2 heterostructure on the nickel foam substrate was evaluated in 1 M KOH at 205 mV of overpotential (as shown in Fig. 5D) for more than 10 h, indicating superior electrochemical HER stability. This outperformed activity is comparable to those described in Co-based electrocatalysts performance and other recently reported transition metal based bifunctional OER and HER catalysts which are depicted in Table S2 in ESI.

3.2.3. *Mechanistic insight besides the catalytic activity of Co_3O_4/MoS_2*

In general, the catalytic activity of Co_3O_4/MoS_2 heterostructure catalyst mainly originates from the surface redox activity of the two pairs of Co (II) and Co (III) and the oxidation of Co (III) to Co (IV) species in the Co_3O_4 respectively [72]. Oxidation current of Co_3O_4/MoS_2 heterostructure is higher than that of Co_3O_4 over the potential ranges, suggesting its higher electrochemical surface area by the MoS_2 on the Co_3O_4 surface. Moreover, MoS_2 support substantial and sufficient adsorptions of oxygen-containing reactive intermediates for the OER on Co (IV) species which are more responsible for the active catalyst center in the OER. Hence, enhanced OER catalytic activity was observed that compared to the counter of Co_3O_4 in alkaline medium. Apart from that, the different atomic planes of Co_3O_4 will fluctuate with respect to the OER catalytic activity [73]. This improvement serves as the basis for the development of intricate Co_3O_4 for enhanced OER activity [30]. Furthermore, the integrated Co_3O_4/MoS_2 heterostructure consisted of Co_3O_4 nano leaves decorated MoS_2 nanosheets can further promote HER catalytic activity that is similar to OER catalytic activity because of their exposed active Mo–S edges and a strong electrostatic attraction of positive Co atoms, negative S atom in the MoS_2. The difference in the electronegativity of S and O induces the faster charge transfer between the components, which can facilitate the fast kinetics of electrochemical performance and it is similar to the recent report of cobalt coupled with Mo_2C [74,75]. Liu et al. reported the heterostructure electronic interaction between Co_3O_4 and MoS_2 is confirmed

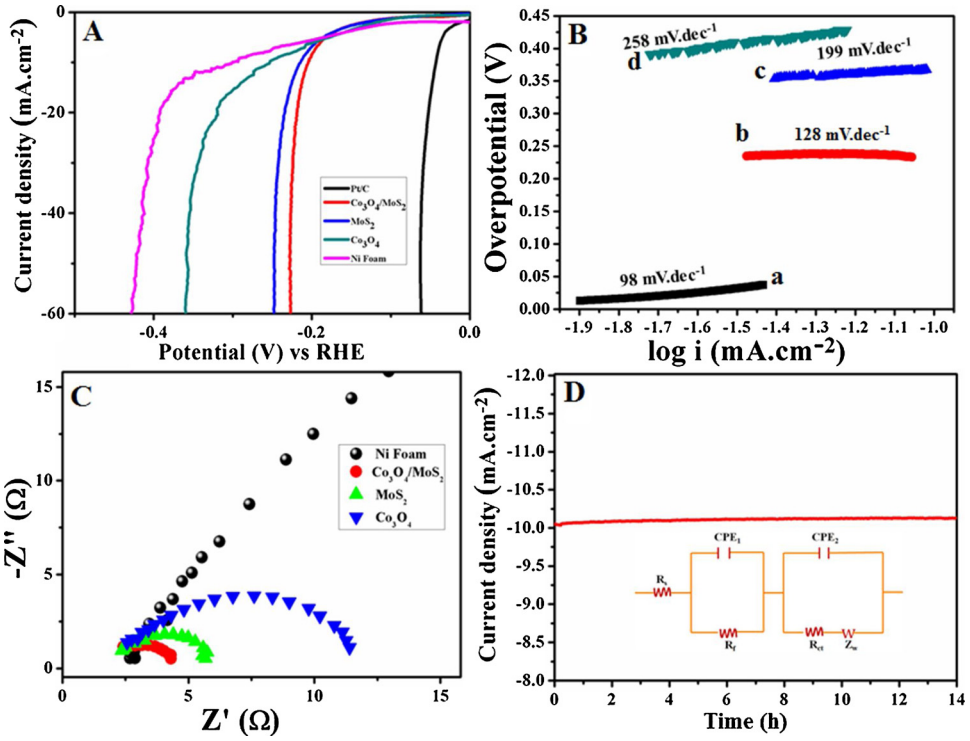

Fig. 5. (A) LSV curves of Pt/C, Co_3O_4 /MoS_2, MoS_2, Co_3O_4, and Ni foam for HER catalysts in 1.0 M KOH solution. (B) Corresponding Tafel plots of the data derived from (A) whereas a) Co_3O_4/MoS_2, b) MoS_2 c) Co_3O_4 and d) Ni foam. (C) EIS plots of different catalyst electrodes at 100 mV of over potential. (D) CA plot of the Co_3O_4/MoS_2 heterostructure electrode at a constant over potential of 205 mV. Inset image is the fitted equivalent circuit model.

by using Bader charge analysis. The charge distribution results stated that the initial electrochemical oxidation of water for HER kinetic is slow for bare MoS_2 nanosheet under the alkaline condition, after constructing with heterostructure of Co_3O_4/MoS_2, hydroxyl (OH^-) ions adsorbing active site was dramatically increased because of Co atom. Hence, electrocatalytic activity towards both OER and HER increases when compared to single phase [68]. Ramas et, al projected the density functional theory of Co_9S_8/MoS_2 heterostructure analysis revealed that the creation of surface vacancy sites on Mo atom strongly interact with Co atom results the formation of stable Co-Mo bonds, these strong bond formation helps the effective electron transfer via sulfur atom intermediate between the Co and Mo metals. The active adjoining phase interaction probably enhances the electron transfer, which leads to higher the electrocatalytic activity of MoS_2 [76,69]. Besides, some of the recent reports showed the transition metal such as Co and Ni-doped MoS_2 can promote structural and electronic modulation to increase the catalytic activity. These strong electronic coupling of Co-MO bond promotes the dissociation of water molecules into H* and OH^- species at the heterostructure due to the strong affinity of OH^- ion at Co site. Likewise, MoS_2 nanosheet effectively adsorbed H* and recombine to forming H_2 molecules [77]. Subsequently, synergy within the Co_3O_4 /MoS_2 heterostructure over the Ni foam develops high-performance electrocatalysts for overall water splitting reaction in the alkaline medium [78–83]. Since, higher electrical conductivity, binder-free attachment of Co_3O_4/MoS_2 over the Ni foam, porous architecture enabled higher adsorption/desorption of reactive intermediates and mass diffusion. To further verify the above postulate, O 1 s XPS spectra of Co_3O_4 /MoS_2 heterostructure was tested before and after the cycling test as shown in (Fig. S9 in ESI) and corresponding binding energy of 533.7 eV can be matched with an OH^- functional group or adsorbed OH^- radical. Noticeably, the intensity of the OH^- functional group is increased after the cycling. Which is 1.5 times higher than that of before cycling test. The obtained results strongly supported the Co_3O_4 /MoS_2 heterostructure large number of OH^- radical adsorbed on the surface of heterostructure and increase the OH^- adsorption for the electrochemical water oxidation reaction [69].

4. Conclusions

In summary, an integrated Co_3O_4/MoS_2 heterostructure electrocatalyst was successfully achieved via facile liquid-phase deposition of MOF followed by a hydrothermal process. Co_3O_4/MoS_2 heterostructure consisting of MOF based Co_3O_4 nano leaves are evenly decorated with layers of MoS_2 nanosheet leading to well-exposed hetero-interface as well as more active sites. The formation of heterointerface is possible due to the strong electrostatic interaction between the positively charged Co_3O_4 nano leaves and negatively charged MoS_2 nanosheet. This unique heterostructure on the Ni foam substrate acts as a bifunctional electrode and can be designed to boost the electrochemical performance towards overall water splitting reaction such as OER and HER electrocatalysts. Such outperform catalytic activity of Co_3O_4/MoS_2 heterostructure could be attributed to the chemisorption of H^+ and OH^- containing intermediates to the interface. Moreover, the layered structure of MoS_2 not only facilitate the intercalation of OH^- ion but also provide fast ion transportation and shorten the diffusion pathway, which can facilitate the reaction kinetics of the overall water splitting process. This work will promote valuable route for designing new materials for application in other fields.

Acknowledgements

Authors acknowledge National Research Foundation of Korea (NRF) grant funded by the Korea government (MISP) (Grant number 2014R1A4A1008140) and the program for fostering next-generation researchers in the engineering of National Research Foundation of Korea (NRF) funded by the Ministry of Education ICT (Grant number 2017H1D8A2030449).

Appendix A. Supplementary data

Supplementary material related to this article can be found, in the online version, at doi:https://doi.org/10.1016/j.apcatb.2019.02.014.

References

[1] H. Zhu, J. Zhang, R. Yanzhang, M. Du, Q. Wang, G. Gao, J. Wu, G. Wu, M. Zhang, B. Liu, J. Yao, X. Zhang, When cubic cobalt sulfide meets layered molybdenum disulfide: a core-shell system toward synergetic electrocatalytic water splitting, Adv. Mater. 27 (2015) 4752–4759.

[2] H. Bin Wu, X.W. (David) Lou, Metal-organic frameworks and their derived materials for electrochemical energy storage and conversion: promises and challenges, Sci. Adv. 3 (2017) 9252.

[3] Y. Li, S. Niu, D. Rakov, Y. Wang, M. Cabán-Acevedo, S. Zheng, B. Song, P. Xu, Metal-organic framework-derived CoPS/N-doped carbon for efficient electrocatalytic hydrogen evolution, Nanoscale 3 (2018) 7291–7297.

[4] J. Kim, D.H. Youn, K. Kawashima, J. Lin, H. Lim, C.B. Mullins, An active nanoporous Ni(Fe) OER electrocatalyst via selective dissolution of Cd in alkaline media, Appl. Catal. B: Environ. 225 (2018) 1–7.

[5] D. Escalera-López, Y. Niu, S.J. Park, M. Isaacs, K. Wilson, R.E. Palmer, N.V. Rees, Hydrogen evolution enhancement of ultra-low loading, size-selected molybdenum sulfide nanoclusters by sulfur enrichment, Appl. Catal. B: Environ. 235 (2018) 84–91.

[6] M.R. Gao, J.X. Liang, Y.R. Zheng, Y.F. Xu, J. Jiang, Q. Gao, J. Li, S.H. Yu, An efficient molybdenum disulfide/cobalt diselenide hybrid catalyst for electrochemical hydrogen generation, Nat. Commun. 6 (2015) 1–7.

[7] H. Wang, S. Min, C. Ma, Z. Liu, W. Zhang, Q. Wang, D. Li, Y. Li, S. Turner, Y. Han, H. Zhu, E. Abou-Hamad, M.N. Hedhili, J. Pan, W. Yu, K.W. Huang, L.J. Li, J. Yuan, M. Antonietti, T. Wu, Synthesis of single-crystal-like nanoporous carbon membranes and their application in overall water splitting, Nat. Commun. 8 (2017) 1–9.

[8] Q. Xu, H. Jiang, H. Zhang, Y. Hu, C. Li, Heterogeneous interface engineered atomic configuration on ultrathin $Ni(OH)_2/Ni_3S_2$ nanoforests for efficient water splitting, Appl. Catal. B: Environ. 242 (2019) 60–66.

[9] Y. Li, K. Yin, L. Wang, X. Lu, Y. Zhang, Y. Liu, D. Yan, Y. Song, S. Luo, Engineering MoS_2 nanomesh with holes and lattice defects for highly active hydrogen evolution reaction, Appl. Catal. B: Environ. 239 (2018) 537–544.

[10] C.C.L. McCrory, S. Jung, I.M. Ferrer, S.M. Chatman, J.C. Peters, T.F. Jaramillo, Benchmarking hydrogen evolving reaction and oxygen evolving reaction electrocatalysts for solar water splitting devices, J. Am. Chem. Soc. 137 (2015) 4347–4357.

[11] J. Zhang, T. Wang, D. Pohl, B. Rellinghaus, R. Dong, S. Liu, X. Zhuang, X. Feng, Interface engineering of MoS_2/Ni_3S_2 heterostructures for highly enhanced electrochemical overall-water-Splitting activity, Angew. Chem. Int. Ed. Engl. 128 (2016) 6814–6819.

[12] H. Wang, H.W. Lee, Y. Deng, Z. Lu, P.C. Hsu, Y. Liu, D. Lin, Y. Cui, Bifunctional non-noble metal oxide nanoparticle electrocatalysts through lithium-induced conversion for overall water splitting, Nat. Commun. 6 (2015) 1–8.

[13] T. Reier, M. Oezaslan, P. Strasser, Electrocatalytic oxygen evolution reaction (OER) on Ru, Ir, and pt catalysts: a comparative study of nanoparticles and bulk materials, ACS Catal. 2 (2012) 1765–1772.

[14] J. Wang, W. Cui, Q. Liu, Z. Xing, A.M. Asiri, X. Sun, Recent progress in cobalt-based heterogeneous catalysts for electrochemical water splitting, Adv. Mater. 28 (2016) 215–230.

[15] A. Aijaz, J. Masa, C. Rossler, W. Xia, P. Weide, A.J.R. Botz, R.A. Fischer, W. Schuhmann, M. Muhler, $Co@Co_3O_4$ encapsulated in carbon nanotube-grafted nitrogen-doped carbon polyhedra as an advanced bifunctional oxygen electrode, Angew. Chemie - Int. Ed. 55 (2016) 4087–4091.

[16] J. Zhou, Y. Dou, A. Zhou, R.M. Guo, M.J. Zhao, J.R. Li, MOF template-directed fabrication of hierarchically structured electrocatalysts for efficient oxygen evolution reaction, Adv. Energy Mater. 7 (2017) 1–10.

[17] M. Gong, H. Dai, A mini-review of NiFe-based materials as highly active oxygen evolution reaction electrocatalysts, Nano Res. 8 (2014) 23–39.

[18] W. Zhou, X.J. Wu, X. Cao, X. Huang, C. Tan, J. Tian, H. Liu, J. Wang, H. Zhang, Ni_3S_2 nanorods/Ni foam composite electrode with low overpotential for electrocatalytic oxygen evolution, Energy Environ. Sci. 6 (2013) 2921.

[19] R. Miao, B. Dutta, S. Sahoo, J. He, W. Zhong, S.A. Cetegen, T. Jiang, S.P. Alpay, S.L. Suib, Mesoporous iron sulfide for highly efficient electrocatalytic hydrogen evolution, J. Am. Chem. Soc. 139 (2017) 13604–13607.

[20] F. Wang, Y. Li, T.A. Shifa, K. Liu, F. Wang, Z. Wang, P. Xu, Q. Wang, J. He, Selenium-enriched nickel selenide nanosheets as a robust electrocatalyst for hydrogen generation, Angew. Chemie - Int. Ed. 55 (2016) 6919–6924.

[21] C. Tang, N. Cheng, Z. Pu, W. Xing, X. Sun, NiSe nanowire film supported on nickel foam : an efficient and stable 3D bifunctional electrode for full water splitting, Angew. Chem. Int. Ed. Engl. (2015) 9483–9487.

[22] J. Huang, Y. Sun, Y. Zhang, G. Zou, C. Yan, S. Cong, T. Lei, X. Dai, J. Guo, R. Lu, Y. Li, J. Xiong, A new member of electrocatalysts based on nickel metaphosphate nanocrystals for efficient water oxidation, Adv. Mater. 30 (2018) 1–9.

[23] Y. Li, C. Zhao, Iron-doped nickel phosphate as synergistic electrocatalyst for water oxidation, Chem. Mater. 28 (2016) 5659–5666.

[24] H. Kim, J. Park, I. Park, K. Jin, S.E. Jerng, S.H. Kim, K.T. Nam, K. Kang, Coordination tuning of cobalt phosphates towards efficient water oxidation catalyst, Nat. Commun. 6 (2015) 1–11.

[25] Y.L. Wang, T. Nie, Y.H. Li, X.L. Wang, L.R. Zheng, A.P. Chen, X.Q. Gong, H.G. Yang, Black tungsten nitride as a metallic photocatalyst for overall water splitting operable at up to 765 nm, Angew. Chemie - Int. Ed. 56 (2017) 7430–7434.

[26] A. Wu, Y. Xie, H. Ma, C. Tian, Y. Gu, H. Yan, X. Zhang, G. Yang, H. Fu, Integrating the active OER and HER components as the heterostructures for the efficient overall water splitting, Nano Energy 44 (2018) 353–363.

[27] J. Ehrmaier, T.N.V. Karsili, A.L. Sobolewski, W. Domcke, Mechanism of photocatalytic water splitting with graphitic carbon nitride: photochemistry of the heptazine-water complex, J. Phys. Chem. A 121 (2017) 4754–4764.

[28] K. Fan, H. Chen, Y. Ji, H. Huang, P.M. Claesson, Q. Daniel, B. Philippe, H. Rensmo, F. Li, Y. Luo, L. Sun, Nickel-vanadium monolayer double hydroxide for efficient electrochemical water oxidation, Nat. Commun. 7 (2016) 1–9.

[29] Z. Zheng, L. Lin, S. Mo, D. Ou, J. Tao, R. Qin, X. Fang, N. Zheng, Economizing production of diverse 2D layered metal hydroxides for efficient overall water splitting, Small 14 (2018) 1800759.

[30] J.A. Koza, Z. He, A.S. Miller, J.A. Switzer, Electrodeposition of crystalline Co_3O_4 - A catalyst for the oxygen evolution reaction, Chem. Mater. 24 (2012) 3567–3573.

[31] Y. Zhao, S. Chen, B. Sun, D. Su, X. Huang, H. Liu, Y. Yan, K. Sun, G. Wang, Graphene-Co_3O_4 nanocomposite as electrocatalyst with high performance for oxygen evolution reaction, Sci. Rep. 5 (2015) 7629.

[32] A.L. Wang, H. Xu, G.R. Li, NiCoFe layered triple hydroxides with porous structures as high-performance electrocatalysts for overall water splitting, ACS Energy Lett. 1 (2016) 445–453.

[33] X. Wang, W. Li, D. Xiong, D.Y. Petrovykh, L. Liu, Bifunctional nickel phosphide nanocatalysts supported on carbon Fiber paper for highly efficient and stable overall water splitting, Adv. Funct. Mater. 26 (2016) 4067–4077.

[34] N. Jiang, B. You, M. Sheng, Y. Sun, Electrodeposited cobalt-phosphorous-Derived films as competent bifunctional catalysts for overall water splitting, Angew. Chem. - Int. Ed. 54 (2015) 6251–6254.

[35] L. Jiao, Y. Wang, H.L. Jiang, Q. Xu, Metal-organic frameworks as platforms for catalytic applications, Adv. Mater. 1703663 (2017) 1–23.

[36] R.B. Lin, S.Y. Liu, J.W. Ye, X.Y. Li, J.P. Zhang, Photoluminescent metal-organic frameworks for gas sensing, Adv. Sci. 3 (2016) 1–20.

[37] J. Qiu, X. Zhang, Y. Feng, X. Zhang, H. Wang, J. Yao, Modified metal-organic frameworks as photocatalysts, Appl. Catal. B: Environ. 231 (2018) 317–342.

[38] P.M. Usov, B. Huffman, C.C. Epley, M.C. Kessinger, J. Zhu, W.A. Maza, A.J. Morris, Study of electrocatalytic properties of metal-organic framework PCN-223 for the oxygen reduction reaction, ACS Appl. Mater. Interfaces 9 (2017) 33539–33543.

[39] C. Wang, Z. Xie, K.E. Dekrafft, W. Lin, Doping metal-organic frameworks for water oxidation, carbon dioxide reduction, and organic photocatalysis, J. Am. Chem. Soc. 133 (2011) 13445–13454.

[40] N. Campagnol, E.R. Souza, D.E. De Vos, K. Binnemans, J. Fransaer, Luminescent terbium-containing metal-organic framework films: new approaches for the electrochemical synthesis and application as detectors for explosives, Chem. Commun. (Camb.) 50 (2014) 12545–12547.

[41] M.Y. Masoomi, A. Morsali, P.C. Junk, Rapid mechanochemical synthesis of two new Cd(ii)-based metal-organic frameworks with high removal efficiency of Congo red, CrystEngComm. 17 (2015) 686–692.

[42] N.A. Khan, S.H. Jhung, Synthesis of metal-organic frameworks (MOFs) with microwave or ultrasound: rapid reaction, phase-selectivity, and size reduction, Coord. Chem. Rev. 285 (2015) 11–23.

[43] N.L. Rosi, J. Eckert, M. Eddaoudi, D.T. Vodak, M. O'Keeffe, O.M. Yaghi, Hydrogen storage in microporous metal-organic frameworks, Science 300 (2003) 1127–1129.

[44] A. Rodríguez-Fortea, P. Alemany, S. Alvarez, E. Ruiz, Exchange coupling in halo-bridged dinuclear Cu(II) compounds: a density functional study, Inorg. Chem. 41 (2002) 3769–3778.

[45] V. Stavila, A.A. Talin, M.D. Allendorf, MOF-based electronic and optoelectronic devices, Chem. Soc. Rev. 43 (2014) 5994–6010.

[46] F.M. Zhang, L.Z. Dong, J.S. Qin, W. Guan, J. Liu, S.L. Li, M. Lu, Y.Q. Lan, Z.M. Su, H.C. Zhou, Effect of imidazole arrangements on proton-conductivity in metal-organic frameworks, J. Am. Chem. Soc. 139 (2017) 6183–6189.

[47] L. Liu, Y. Zhou, S. Liu, M. Xu, The applications of metal-organic frameworks in electrochemical sensors, ChemElectroChem 5 (2018) 6–19, https://doi.org/10.1002/celc.201700931.

[48] M. Jahan, Z. Liu, K.P. Loh, A graphene oxide and copper-centered metal-organic framework composite as a tri-functional catalyst for HER, OER, and ORR, Adv. Funct. Mater. 23 (2013) 5363–5372.

[49] B. Xiong, L. Chen, J. Shi, Anion-containing noble-metal-Free bifunctional electrocatalysts for overall water splitting, ACS Catal. 8 (2018) 3688–3707.

[50] L. Hu, Y. Huang, F. Zhang, Q. Chen, CuO/Cu_2O composite hollow polyhedrons fabricated from metal–organic framework templates for lithium-ion battery anodes with a long cycling life, Nanoscale 5 (2013) 4186–4190.

[51] S. Xiao, D. Pan, R. Liang, W. Dai, Q. Zhang, G. Zhang, C. Su, H. Li, W. Chen, Bimetal MOF derived mesocrystal $ZnCo_2O_4$ on rGO with High performance in visible-light photocatalytic NO oxidization, Appl. Catal. B: Environ. 236 (2018) 304–313.

[52] Y. Yang, K. Zhang, H. Lin, X. Li, H.C. Chan, L. Yang, Q. Gao, MoS_2–Ni_3S_2 heteronanorods as efficient and stable bifunctional electrocatalysts for overall water splitting, ACS Catal. 7 (2017) 2357–2366.

[53] J. Liu, Y. Liu, D. Xu, Y. Zhu, W. Peng, Y. Li, F. Zhang, X. Fan, Hierarchical "nanoroll" like $MoS_2/Ti_3C_2T_x$ hybrid with high electrocatalytic hydrogen evolution activity, Appl. Catal. B: Environ. 241 (2019) 89–94.

[54] J. Zhang, T. Wang, P. Liu, S. Liu, R. Dong, X. Zhuang, M. Chen, X. Feng, Engineering water dissociation sites in MoS_2 nanosheets for accelerated electrocatalytic hydrogen production, Energy Environ. Sci. 9 (2016) 2789–2793.

[55] S. Shin, Z. Jin, D.H. Kwon, R. Bose, Y.S. Min, High turnover frequency of hydrogen evolution reaction on amorphous MoS_2 thin film directly grown by atomic layer deposition, Langmuir 31 (2015) 1196–1202.

[56] J. Wang, D. Chao, J. Liu, L. Li, L. Lai, J. Lin, Z. Shen, $Ni_3S_2@MoS_2$core/shell nanorod arrays on Ni foam for high-performance electrochemical energy storage, Nano Energy 7 (2014) 151–160.

[57] S. Reddy, R. Du, L. Kang, N. Mao, J. Zhang, Three-dimensional CNTs aerogel/MoS_x as an electrocatalyst for hydrogen evolution reaction, Appl. Catal. B: Environ. 194 (2016) 16–21.

[58] S. Jing, L. Zhang, L. Luo, J. Lu, S. Yin, P.K. Shen, T. Panagiotis, N-doped porous molybdenum Carbide Nanobelts as efficient catalysts for hydrogen evolution reaction, Appl. Catal. B: Environ. 224 (2018) 533–540.
[59] Y. Liu, X. Xu, J. Zhang, H. Zhang, W. Tian, X. Li, M.O. Tade, H. Sun, S. Wang, Flower-like MoS_2 on graphitic carbon nitride for enhanced photocatalytic and electrochemical hydrogen evolutions, Appl. Catal. B: Environ. 239 (2018) 334–344.
[60] Y. Yan, B.Y. Xia, B. Zhao, X. Wang, A review on noble-metal-free bifunctional heterogeneous catalysts for overall electrochemical water splitting, J. Mater. Chem. A Mater. Energy Sustain. 4 (2016) 17587–17603.
[61] Y. Yang, W. Zhang, Y. Xiao, Z. Shi, X. Cao, Y. Tang, Q. Gao, $CoNiSe_2$ heteronanorods decorated with layered-double-Hydroxides for efficient hydrogen evolution, Appl. Catal. B: Environ. 242 (2019) 132–139.
[62] P. Tan, B. Chen, H. Xu, W. Cai, W. He, M. Ni, In-situ growth of Co_3O_4 nanowire-assembled clusters on nickel foam for aqueous rechargeable Zn-Co_3O_4 and Zn-air batteries, Appl. Catal. B: Environ. 241 (2019) 104–112.
[63] A. Sivanantham, S. Shanmugam, Nickel selenide supported on nickel foam as an efficient and durable non-precious electrocatalyst for the alkaline water electrolysis, Appl. Catal. B: Environ. 203 (2017) 485–493.
[64] R. Chen, J. Yao, Q. Gu, S. Smeets, C. Baerlocher, H. Gu, D. Zhu, W. Morris, O.M. Yaghi, H. Wang, A two-dimensional zeolitic imidazolate framework with a cushion-shaped cavity for CO_2 adsorption, Chem. Commun. (Camb.) 49 (2013) 9500–9502.
[65] X. Xiong, W. Luo, X. Hu, C. Chen, L. Qie, D. Hou, Y. Huang, Flexible membranes of MoS_2/C nanofibers by electrospinning as binder-free anodes for high-performance sodium-ion batteries, Sci. Rep. 5 (2015) 4–9.
[66] A. Muthurasu, S.V. Sheen Mers, V. Ganesh, Nitrogen-doped graphene quantum dots (N-GQDs)/Co_3O_4 composite material as an efficient bi-functional electrocatalyst for oxygen evolution and oxygen reduction reactions, Int. J. Hydrogen Energy 43 (2018) 4726–4737.
[67] J. Li, G. Lu, G. Wu, D. Mao, Y. Guo, Y. Wang, Y. Guo, Effect of TiO_2 crystal structure on the catalytic performance of Co_3O_4/TiO_2 catalyst for low-temperature CO oxidation, Catal. Sci. Technol. 4 (2014) 1268–1275.
[68] J. Liu, J. Wang, B. Zhang, Y. Ruan, H. Wan, X. Ji, K. Xu, D. Zha, L. Miao, J. Jiang, Mutually beneficial Co_3O_4@MoS_2heterostructures as a highly efficient bifunctional catalyst for electrochemical overall water splitting, J. Mater. Chem. A Mater. Energy Sustain. 6 (2018) 2067–2072.
[69] Q. Xu, H. Jiang, H. Zhang, Y. Hu, C. Li, Heterogeneous interface engineered atomic configuration on ultrathin $Ni(OH)_2$/Ni_3S_2nanoforests for efficient water splitting, Appl. Catal. B Environ. 242 (2019) 60–66.
[70] Y. Yu, J. Zhang, M. Zhong, S. Guo, Co_3O_4 nanosheet arrays on Ni foam as electrocatalyst for oxygen evolution reaction, Electrocatalysis 9 (2018) 653–661.
[71] W. Xiao, P. Liu, J. Zhang, W. Song, Y.P. Feng, D. Gao, J. Ding, Dual-functional N dopants in edges and basal plane of MoS_2 nanosheets toward efficient and durable hydrogen evolution, Adv. Energy Mater. 7 (2017) 1–10.
[72] W. Xu, F. Lyu, Y. Bai, A. Gao, J. Feng, Z. Cai, Y. Yin, Porous cobalt oxide nanoplates enriched with oxygen vacancies for oxygen evolution reaction, Nano Energy 43 (2018) 110–116.
[73] X.L. Xu, Z.H. Chen, Y. Li, W.K. Chen, J.Q. Li, Bulk and surface properties of spinel Co_3O_4 by density functional calculations, Surf. Sci. 603 (2009) 653–658.
[74] W. Ren, H. Zhang, C. Guan, C. Cheng, Ultrathin MoS_2 Nanosheets@Metal organic framework-derived N-Doped carbon nanowall arrays as sodium ion battery anode with superior cycling life and rate capability, Adv. Funct. Mater. 27 (2017) 1–10.
[75] M. Kim, S. Kim, D. Song, S. Oh, K.J. Chang, E. Cho, Promotion of electrochemical oxygen evolution reaction by chemical coupling of cobalt to molybdenum carbide, Appl. Catal. B: Environ. 227 (2018) 340–348.
[76] H. Zhang, H. Jiang, Y. Hu, P. Saha, C. Li, Mo-Triggered amorphous Ni_3 S_2 nanosheets as efficient and durable electrocatalysts for water splitting, Mater. Chem. Front. 2 (2018) 1462–1466.
[77] Q. Xu, Y. Liu, H. Jiang, Y. Hu, H. Liu, C. Li, Unsaturated sulfur edge engineering of strongly coupled MoS_2 nanosheet–Carbon macroporous hybrid catalyst for enhanced hydrogen generation, Adv. Energy Mater. 1802553 (2018) 1–8.
[78] X. Hai, W. Zhou, S. Wang, H. Pang, K. Chang, F. Ichihara, J. Ye, Rational design of freestanding MoS_2 monolayers for hydrogen evolution reaction, Nano Energy 39 (2017) 409–417.
[79] G. Liu, A.W. Robertson, M.M.J. Li, W.C.H. Kuo, M.T. Darby, M.H. Muhieddine, Y.C. Lin, K. Suenaga, M. Stamatakis, J.H. Warner, S.C.E. Tsang, MoS_2 monolayer catalyst doped with isolated Co atoms for the hydrodeoxygenation reaction, Nat. Chem. 9 (2017) 810–816.
[80] D. Escalera-López, Y. Niu, J. Yin, K. Cooke, N.V. Rees, R.E. Palmer, Enhancement of the hydrogen evolution reaction from Ni-MoS_2 hybrid nanoclusters, ACS Catal. 6 (2016) 6008–6017.
[81] L. Yu, B.Y. Xia, X. Wang, X.W. Lou, General formation of M-MoS_3 (M = Co, Ni) hollow structures with enhanced electrocatalytic activity for hydrogen evolution, Adv. Mater. 28 (2016) 92–97.
[82] H. Zhang, L. Yu, T. Chen, W. Zhou, X.W. (David) Lou, Surface Modulation of Hierarchical MoS_2 Nanosheets by Ni Single Atoms for Enhanced Electrocatalytic Hydrogen Evolution, Adv. Funct. Mater. 1807086 (2018) 1–8.
[83] N.H. Attanayake, A.C. Thenuwara, A. Patra, Y.V. Aulin, T.M. Tran, H. Chakraborty, E. Borguet, M.L. Klein, J.P. Perdew, D.R. Strongin, Effect of intercalated metals on the electrocatalytic activity of 1T-MoS_2 for the hydrogen evolution reaction, ACS Energy Lett. 3 (2018) 7–13.